Clin Neuroradiol (2016) 26:391–403
DOI 10.1007/s00062-015-0469-9

REVIEW ARTICLE

Physics, Techniques and Review of Neuroradiological Applications of Diffusion Kurtosis Imaging (DKI)

M. Marrale · G. Collura · M. Brai · N. Toschi · F. Midiri · G. La Tona · A. Lo Casto · C. Gagliardo

Received: 28 July 2015 / Accepted: 22 September 2015 / Published online: 20 November 2015

Abstract In recent years many papers about diagnostic applications of diffusion tensor imaging (DTI) have been published. This is because DTI allows to evaluate *in vivo* and in a non-invasive way the process of diffusion of water molecules in biological tissues. However, the simplified description of the diffusion process assumed in DTI does not permit to completely map the complex underlying cellular components and structures, which hinder and restrict the diffusion of water molecules. These limitations can be partially overcome by means of diffusion kurtosis imaging (DKI). The aim of this paper is the description of the theory of DKI, a new topic of growing interest in radiology. DKI is a higher order diffusion model that is a straightforward extension of the DTI model. Here, we analyze the physics underlying this method, we report our MRI acquisition protocol with the preprocessing pipeline used and the DKI parametric maps obtained on a 1.5 T scanner, and we review the most relevant clinical applications of this technique in various neurological diseases.

Keywords Diffusional kurtosis imaging (DKI) · Diffusion tensor imaging (DTI) · Diffusion weighted imaging (DWI) · Magnetic resonance imaging (MRI) · Neuroradiology · Brain

M. Marrale, PhD (✉) · G. Collura, MSc · Prof. M. Brai
Department of Physics and Chemistry, University of Palermo, Palermo, Italy
e-mail: maurizio.marrale@unipa.it

N. Toschi, PhD
Medical Physics Section, Department of Biomedicine and Prevention, University of Rome "Tor Vergata"
Rome, Italy

N. Toschi, PhD
Department of Radiology, Athinoula A. Martinos Center for Biomedical Imaging
Boston, MA, USA

N. Toschi, PhD
Harvard Medical School
Boston, MA, USA

F. Midiri
University of Palermo
Palermo, Italy

G. La Tona, MD · A. Lo Casto, MD · C. Gagliardo, MD, PhD
Department of Biopathology and Medical Biotechnologies, Section of Radiological Sciences, University of Palermo, Palermo, Italy
e-mail: cesare.gagliardo@unipa.it

An Introduction to Diffusion Kurtosis Imaging

The analysis of diffusion tensor imaging (DTI) allows to evaluate *in vivo* and in a non-invasive way the process of diffusion of water molecules in biological tissues [1]. The peculiar organization of some biological tissues (such as white matter of the central nervous system or tissues with high cellularity) influences this phenomenon making it anisotropic and therefore well evaluable with this technique [2–4]. The combined use of DTI with other advanced neuroimaging techniques has also been implemented in clinical scenarios [5, 6]. Changes in tissue anisotropy can also be found in many diseases before any signal intensity variation on conventional MR pulse sequences (*e.g.* for ischemia see [7]) since they are intimately related to intrinsic microstructural changes [8]. Notwithstanding all these important applications, DTI fails to fully utilize the MR diffusion measurements that are inherent to tissue microstructure. DTI implicitly assumes that water molecule diffusion occurs with a Gaussian distribution of diffusion displacement. This assumption has been experimentally demonstrated to be not suitable in both white matter (WM) and gray matter (GM) when high b-values are used (which, in turn, are essential to probe different diffusion regimes simul-

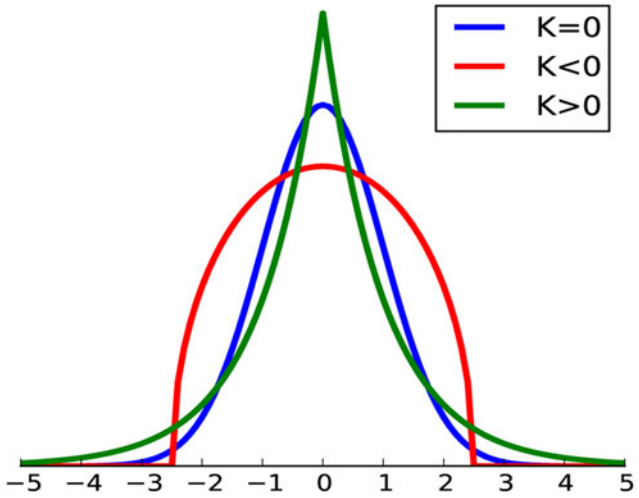

Fig. 1 The three probability densities in the figure have different values of kurtosis: in blue a Gaussian with $K = 0$; in red a curve with $K < 0$; in green a curve with $K > 0$

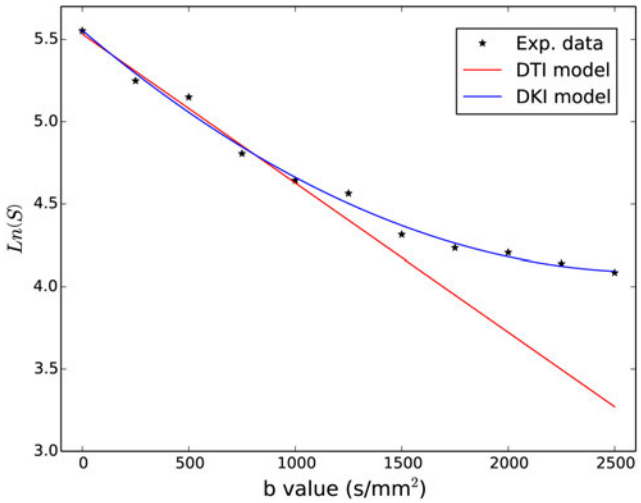

Fig. 2 Example of comparison of the fit of experimental data with DTI model and DKI model. Data taken from cerebral white matter (corticospinal tract)

taneously) [9, 10]. In biological tissue, complex underlying cellular components and structures hinder and restrict the diffusion of water molecules. Moreover, the simplified description of the diffusion process in vivo by a 2nd-order 3D diffusivity tensor prevents DTI from being truly effective in characterizing relatively isotropic tissue such as GM. Even in WM, the DTI model can fail if the tissue contains substantial crossing or diverging fibers [11, 12]. Jensen [13] introduced diffusion kurtosis imaging (DKI), a higher order diffusion model that is a straightforward extension of the DTI model.

The aim of this work is the description of the theory of Diffusion Kurtosis Imaging (DKI) and the MRI protocol we used for DKI acquisitions at 1.5 T. As final step, we also review some of the most relevant clinical applications of this technique in various neurological diseases such as ischemia, mild cognitive impairment (MCI), Alzheimer Disease (AD), Parkinson's Disease (PD) and gliomas.

Theoretical Model

DKI approximates the diffusion-weighted signal attenuation more accurately with respect to DTI, by quantifying the degree of non-Gaussian diffusion. For this purpose, the exponent of the DTI model is extended with a quadratic term in the b-value. The coefficient of the additional term is related to the apparent excess kurtosis (AKC), a dimensionless metric quantifying the non-gaussianity. DKI is an approximation of the logarithmic expansion of the DWI signal decay up to the b^2 term and neglects the b^3 terms. In DKI, the word "Kurtosis" refers to the excess kurtosis that is the normalized and standardized fourth central moment of the water displacement distribution. It is a dimensionless measure that quantifies the deviation of the water diffusion displacement profile from the Gaussian distribution of unrestricted diffusion, providing a measure of the degree of diffusion hindrance or restriction Fig. 1.

In DTI analyses the directionality of diffusion can be expressed by a symmetric tensor of second-order 3×3, $\mathbf{D}$, with six independent components. In DKI analyses the directionality of the kurtosis can be expressed by a symmetric tensor of the fourth order $3 \times 3 \times 3 \times 3$, $\mathbf{W}$. $\mathbf{W}$ being symmetric, among its 81 elements, only 15 are independent. So, in order to estimate $\mathbf{D}$ and $\mathbf{W}$ at the same time, it needs at least two non-zero b-values (besides b = 0) and 21 non-co-linear directions of diffusion gradients.

In order to understand the improvement achieved with DK analysis let us consider the trend of the MRI signal acquired also for b-values larger than 500 s/mm^2 (see Fig. 2). As can be seen from this plot, the DTI model is characterized by a linear curve (in logarithmic scale of signal) for low b-values (smaller than 1000 s/mm^2) that well describes the trend of experimental data whereas for high b-values a deviation from linear trend is observed. On the other hand, the DKI model fits well the data also for b-values larger than 1000 s/mm^2. Indeed, according to the DKI model the dependence of the $S(b, \mathbf{g})$ on the b-value for each direction of the gradient $\mathbf{g}$ is the following:

$$\ln \frac{S(b,\mathbf{g})}{S_0} = -bD_{app}(\mathbf{g}) + \frac{1}{6}b^2 D_{app}(\mathbf{g})^2 K_{app}(\mathbf{g}) \qquad (1)$$

where $D_{app}(\mathbf{g})$ and $K_{app}(\mathbf{g})$ are the apparent diffusion coefficient and the coefficient of apparent kurtosis measured along a direction of specific diffusion $\mathbf{g} = (g_1, g_2, g_3)$, respectively. The relationships between $D_{app}(\mathbf{g})$ and $K_{app}(\mathbf{g})$ and their respective tensors are:

$$D_{app}(\mathbf{g}) = \sum_{i=1}^{3}\sum_{j=1}^{3} g_i g_j D_{ij} \tag{2}$$

$$K_{app}(\mathbf{g}) = \frac{MD^2}{D_{app}(\mathbf{g})^2}\sum_{i=1}^{3}\sum_{j=1}^{3}\sum_{k=1}^{3}\sum_{l=1}^{3} g_i g_j g_k g_l W_{ijkl} \tag{3}$$

where D_{ij} are the elements of $\mathbf{D}$, and W_{ijkl} are the elements of $\mathbf{W}$ and $MD = \frac{1}{3}\sum_{i=1}^{3} D_{ii}$ is the mean diffusivity.

As can be seen from Fig. 2 the DKI model includes a quadratic dependence on b; this dependence is not considered by the simple DTI model which is not able to fit the data for larger values of gradients and, therefore, of b-values for a given diffusion time. The application of suitable fitting procedure allows to extract the values of the elements of $\mathbf{D}$ and $\mathbf{W}$ and from these the characteristic values of the DK analysis. In particular, the diffusion kurtosis along each of the directions of the eigenvectors is related to the eigenvalues λ_1, λ_2, λ_3 of the diffusion tensor:

$$K_i = \frac{MD^2}{\lambda_i^2}\hat{W}_{iiii}. \tag{4}$$

The Mean Kurtosis (MK) is calculated as the average of the kurtosis along all directions of diffusion gradients [14]

$$MK = \frac{1}{N}\sum_{i=1}^{N}(K_{app})_i \tag{5}$$

The axial kurtosis, K_a, and the radial kurtosis, K_r, are calculated similarly to the axial and radial diffusion:

$$K_a = K_1 \tag{6}$$

$$K_r = \frac{K_2 + K_3}{2} \tag{7}$$

which is of interest for white matter bundles since it gives additional information of the axonal and myelin integrity [15]. Previous studies have shown that DKI provides more robust and unbiased data when compared to DTI [16]. In particular, DKI technique uses a larger set of b-values data and is based on a 2nd order approximation of the dependence of signal on b-values and this leads to a more robustness of fitted parameters. Furthermore, as reported by Veerat et al. [17] the parameter estimation with DKI is less b-value dependent than the one obtained through DTI resulting in unbiased data [17, 16]. While with DKI it is mandatory to have good SNR even for high b-values, recent advances in scanner and coil technology have provided access to good quality diffusion weighted imaging at 1.5 T. Also, while higher field intensities are preferable in most modalities, in DW imaging the gain in SNR at high field will have to compete with field-dependent T_2 shortening. It should be noted that a "good" SNR guarantees that the non-linear behavior of the ln $S(b)$ is not due to the noise floor, which is a consequence of Rician noise in the magnitude data [18].

Nowadays, other additional diffusion MRI based frameworks (such as Composite Hindered And Restricted ModEl of Diffusion, CHARMED [19], and ActiveAx [20]) were developed enabling the extraction of a multitude of microstructural parameters (axon diameter distribution, mean axonal diameter and axonal density). However, these techniques are difficult to be used in clinical examinations since they require very long time acquisition (at least 4-5 non-zero b-values and very high b-values which are not always available in a clinical diagnostic setting especially when using 1.5 T scanners). Recently, also a technique for Neurite Orientation Dispersion and Density Imaging (NODDI) [21] has been developed. This technique requires at least 2 non-zero b-values (the same number as DKI); however, the DKI technique could be more sensitive than NODDI (even though less specific) because DKI is a technique without biophysical assumptions whereas NODDI is characterized by a model which separates the fibers from extra-cellular component [21].

It must be underlined that the extensive application of DKI in a clinical-experimental scenario must deal with several difficulties. The most important is the long acquisition time (much more time than that required for the DTI). In practice, in both DTI and DKI, more data are acquired than the minimum required in order to improve the robustness of the reconstruction procedure.

One typical scheme of a DKI sequence with 30 directions of diffusion gradients and 5 non-zero different b-values (500, 1000, 1500, 2000, 2500 s/mm^2) requires an acquisition time of about 20 min for a whole-brain study. Recently it has been proposed a scheme with a shorter acquisition time. This scheme includes the acquisition of 30 gradients directions and two non-zero b-values (1000 and 2000 s/mm^2) which takes about 7 min for a whole brain coverage [22]. In clinical applications the real issues is to find a good compromise between acquisition time and robustness of the fit. More measurements may correspond to more b-values or more directions of the gradients, but each type of algorithm, in principle, will respond differently to different types of acquisition schemes.

Another major problem of DKI is that these DWI images are usually acquired with an echo planar imaging (EPI) sequence and also require high b-values, resulting in a low SNR of acquired diffusion weighted images. Distortion correction is an important step in DKI. However, in order to become a routine procedure, DKI still needs to be improved in terms of robustness, reliability, and reproducibility. The lack of standard procedures for post-processing, especially for noise correction, might become a significant issue for the

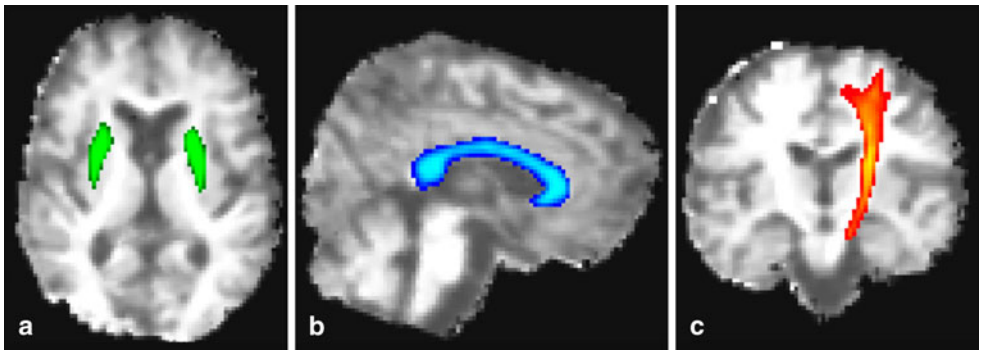

Fig. 3 Anatomical region of interest (ROI) were identified on MK maps by superimposing structure's probability map from the Juelic Histological Atlas for white matter bundles and Harvard-Oxford Subcortical Structural Atlas for deep grey matter structures. (**a**) bilateral putamen nuclei. (**b**) sagittal multi-planar reconstruction (MPR) with the superimposed atlas' corpus callosum (blue). (**c**) coronal MPR with the superimposed atlas' left cortical spinal tract (orange)

use of DKI in clinical routine. Almost all of the published works are carried out with high-field (3 T) MR scanners, there are few experiments carried out with most widely installed MRI units for clinical applications (1.5 T scanners) and the majority of these are preliminary experiments on phantoms (*e.g.* see [23]).

Example of Imaging Acquisition

In our preliminary experience, MRI images were acquired using a 1.5 T Philips-Achieva (Philips Healthcare, Best, the Netherlands) with a 8-channel head coil.

Acquisition Parameters

Whole brain T_2-weighted fat-sat images were acquired with TR = 15324.3 ms, TE = 110 ms, matrix = 100×85, FOV = 200×200 mm^2, slices per slab = 65, slice thickness = 1.8 mm, slices gap=1.8 mm, bandwidth = 152 Hz/pixel NEX = 4 in a total time of 5.35 min. Diffusion-weighted images were acquired along 32 gradient directions for b = 0, 1000, 2000 mm^2 with a single shot spin-echo imaging sequence [24] with TR = 7000 ms, TE = 130 ms, matrix = 80×80, FOV = 240×240 mm^2, slices = 40, slice thickness = 3 mm, no gap, NEX = 4 for b = 0, NEX = 1 for b = 1000, 2000 s/mm^2, bandwidth = 2681 Hz/pixel; total acquisition time = 7.81 min. The protocol acquisition time was about 30 min including isotropic 3D Fluid Attenuation Inversion Recovery (FLAIR) and 3D T_1 Turbo Field Echo (TFE) for obtaining the other clinical information.

Analysis of the MRI Data

A mask was created to remove non-brain matter from analysis using FSL's Brain Extraction Tool (BET) applied on b0 image (http://www.fmrib.ox.ac.uk/fsl/). Diffusion data were offline processed using the standard TORTOISE processing pipeline: DWIs were corrected for motion and eddy current distortions and EPI distortion. T2-FSE images were used as the structural target [25] (https://science.nichd.nih.gov/confluence/display/nihpd/TORTOISE). The data analysis was performed using in-house developed software implemented in Python (https://www.python.org/) as described in [26].

DKI Images

The DKI protocol used in this work allowed to obtain images whose content in terms of the typical parameters of the DKI is comparable with those reported in literature [27] by performing, for example, a ROI-based analysis (*e.g.* frontal white matter, corpus callosum, cortico-spinal tracts, and deep grey matter) (Fig. 3). Typical parametric maps obtained from our datasets (Fig. 4) have a good spatial and contrast resolution for experimental future diagnostic applications as confirmed by in house experienced radiologists. In our experience, these parameters are suitable for a 1.5 T scanner and represent a good compromise between acquisition time for clinical acquisitions and robustness of the data.

Neuroradiological Applications

Diffusion-weighted imaging can provide physiologic information about healthy and diseased brain tissues [28–31]. Conventional diffusion-weighted imaging and DTI imaging techniques assume a Gaussian diffusion distribution [32]. DKI imaging is a recently developed method that can measure non-Gaussian diffusion, thereby being possibly more

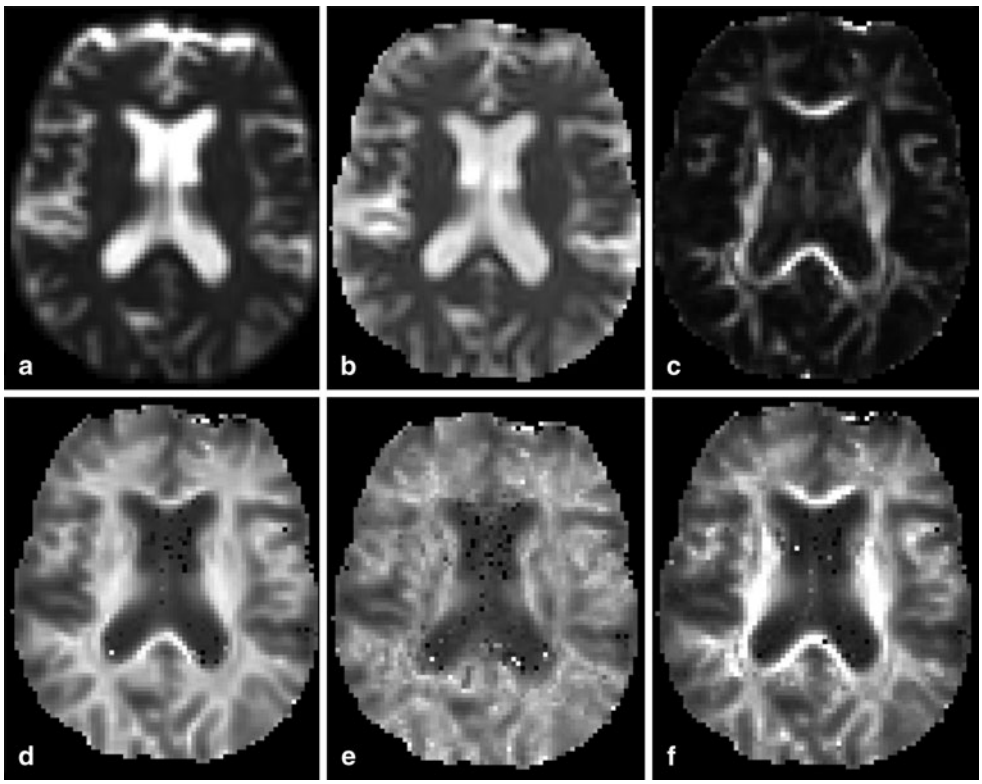

Fig. 4 Isotropic ($3 \times 3 \times 3\ mm^3$) parametric maps for the diffusion metrics of b0 (**a**), MD (**b**), FA(**c**), MK (**d**), Ka (**e**), and Kr (**f**) from a DKI dataset. No spatial smoothing filter has been applied

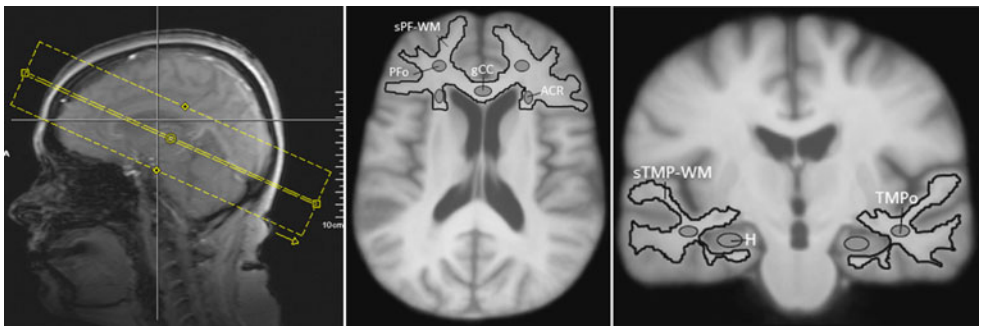

Fig. 5 Manually drawn and automatically generated regions-of-interest (ROIs) used to compare the diffusion metrics between subject groups by Falangola et al. [37]. Segmented prefrontal white matter (sPF-WM); prefrontal oval (PFo); genu of the corpus callosum (gCC); anterior corona radiata (ACR); segmented temporal white matter (sTMP-WM); temporal oval (TMPo); hippocampus (H). Reproduced from Falangola et al. [37] with permission of Elsevier Inc

suitable than conventional DTI imaging for the detection of micro-structural changes [33].

One of the first applications of DWI images is the acute cerebral ischemia [34]. Even though conventional DWI is deemed to be the most reliable method for stroke imaging in clinical practice, the nature of conventional diffusion metrics is strongly compromised by partial volume contamination from free fluid as a result of, for example, vasogenic edema during the subacute phase compared to DKI [35]. Studying a population of patients who underwent MRI 6 h to 2 weeks after symptom onset, Hui et al. showed by the use of DKI metrics that ischemia has a larger effect on the intra- than the extra-axonal environments and this observation looks consistent with focal enlargement of axons and dendrites as a result of osmotic imbalance (axonal swelling or beading) [36]. The DKI imaging method can be helpful in the detection of tissue microstructure changes by revealing distinct ischemic lesion signal heterogeneity on MK that is not apparent on MD maps from DTI datasets. Even if a small number of hypointense voxels on the MK maps are likely attributable to poor model fitting rather than actual microstructural features the image clearly shows the gain obtained from the use of sequences DKI in the identification of parenchymal heterogeneity in cases of cerebral ischemia [36]. In next future additional

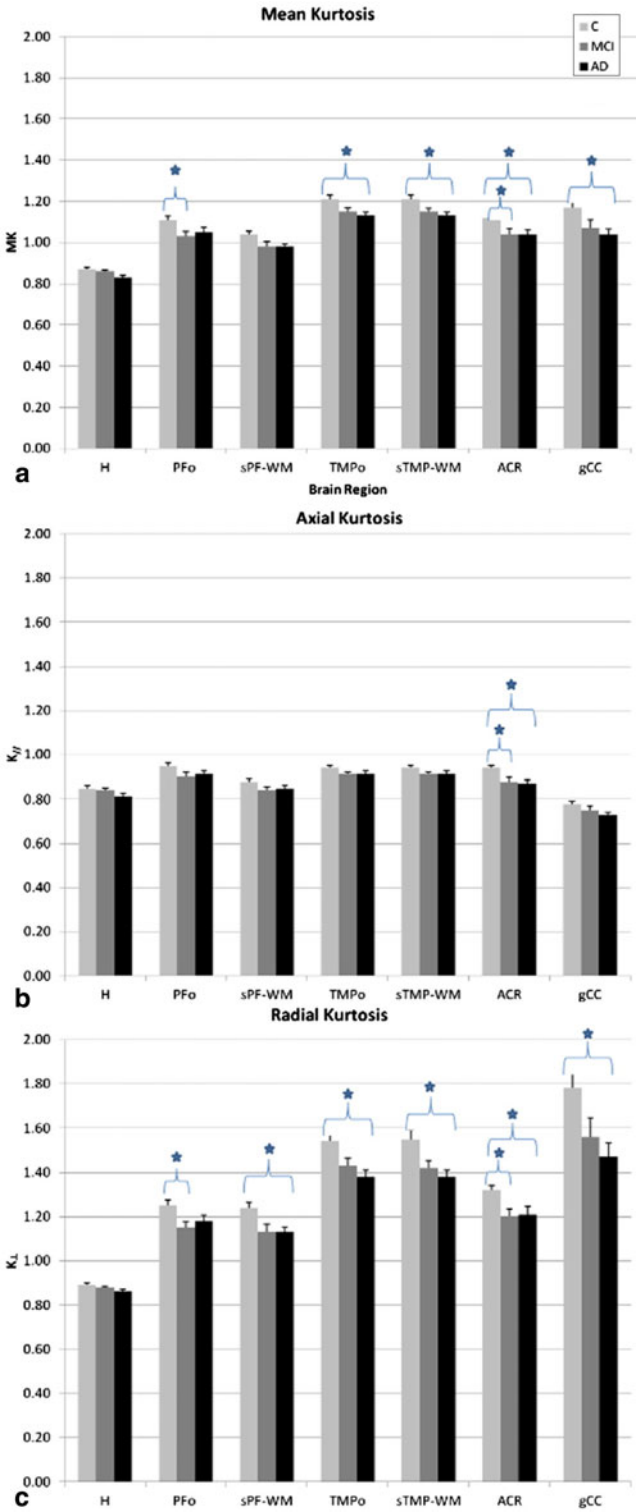

Fig. 6 Mean values (± SDs) of the DK metrics for the three groups (control, MCI and AD) for each ROI (see Fig. 5): (**a**) Mean Kurtosis, (**b**) Axial kurtosis, (**c**) Radial kurtosis; the indices that were found to be statistically significant after Tukey's multiple comparison correction are highlighted. Relative to the control group, AD patients showed significant mean, axial and radial diffusivity increases in all brain regions examined. No statistically significant fractional anisotropy differences were found in any of the ROIs, but AD patients showed a trend towards reduced fractional anisotropy in all white matter regions examined and in the hippocampus. When comparing AD and MCI groups only in the hippocampus the mean, axial and radial diffusivity values were significantly increased. Relative to the control group, the MCI group showed significantly increased mean diffusivity in the PFo and radial diffusivity in the PFo and ACR. Reproduced from Falangola et al. [37] with permission of Elsevier Inc

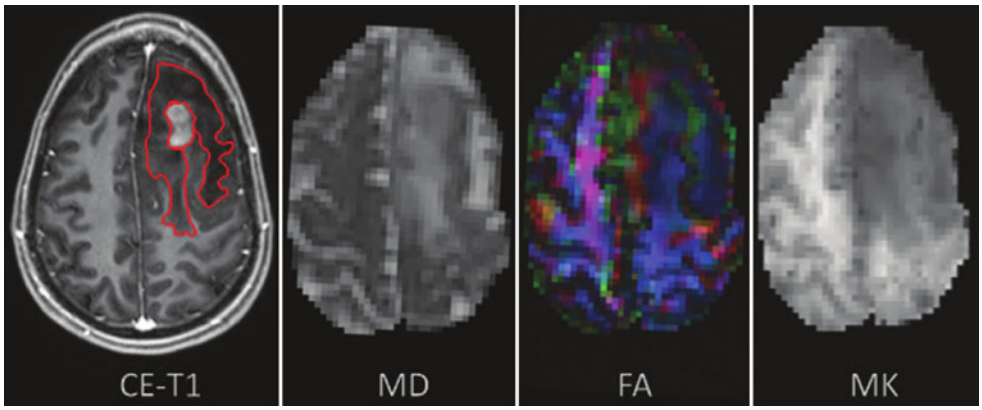

Fig. 7 Transverse contrast-enhanced T_1-weighted (CE-T_1) image, MD map, FA map, and mean kurtosis (MK) map in 30-year-old woman with a low-grade glioma that showed focal progression to a high-grade glioma. The mean kurtosis map shows the differences between the malignant part of the tumor (high mean kurtosis values, approaching the values of white matter) and the low-grade tumor (low mean kurtosis values). Reproduced from Van Cauter et al. [44] with permission of Radiological Society of North America

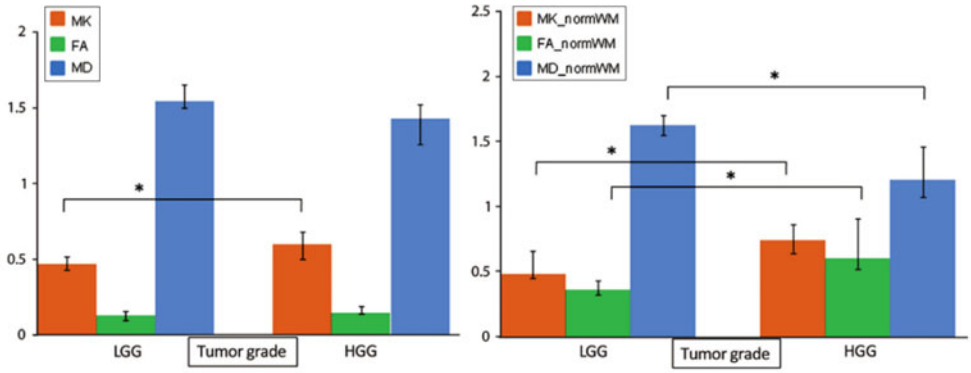

Fig. 8 Left: Bar graph shows MK, FA, and MD in low-grade gliomas (LGG) and high-grade gliomas (HGG). Right: Bar graph shows parameters in solid tumor normalized to the age-corrected value in the contralateral normal appearing white matter (NAWM, shown as "_normWM" in picture). On the *y*-axis the values of various parameters are reported: MD is given in 10^{-3} mm^2/sec, the remaining parameters are dimensionless. Error bars = interquartile ranges. $*$ = Statistically significant difference ($P < 0.05$, Bonferroni corrected). Reproduced from Van Cauter et al. [44] with permission of Radiological Society of North America

imaging-based information on the physiopathological mechanisms behind neuronal injury in brain ischemia could for example open new approaches to therapy in patients eligible to tissue-type plasminogen activator treatment.

In the last decades DTI has been used to investigate brain microstructure changes in PD [13, 38–41] but the results of these studies are still controversial. The anterior cingulum is a part of the brain in which pathological alterations occur relatively early in PD, and diffusion abnormalities in cingulate fibers have been reported in some DTI study [13, 38, 39]. Recently Kamagata et al. examined the cingulate fibers by using DKI and they found that MK and FA in the anterior cingulum were significantly lower in PD patients than in healthy controls [42]. Authors also found that the best diagnostic performance was achieved by analyzing MK values in the anterior cingulum suggesting this region of interest as a useful biomarker for the early diagnosis of PD [42]. Furthermore Wang et al. has compared the MK, FA, and mean, axial, and radial diffusivity of the basal ganglia proving that the characterization of non-Gaussian water diffusion with use of DKI, as compared with conventional imaging, can lead to a substantial improvement in the clinical MR imaging of PD [43].

Tissue micro-structural changes where also found in neurodegenerative disorders. Patients with mild cognitive impairment (MCI) and Alzheimer Disease (AD) showed statistically significant difference in kurtosis parameters as compared to cognitively intact controls (C) in selected brain regions (segmented prefrontal white matter, sPF-WM; prefrontal oval, PFo; genu of the corpus callosum, gCC; anterior corona

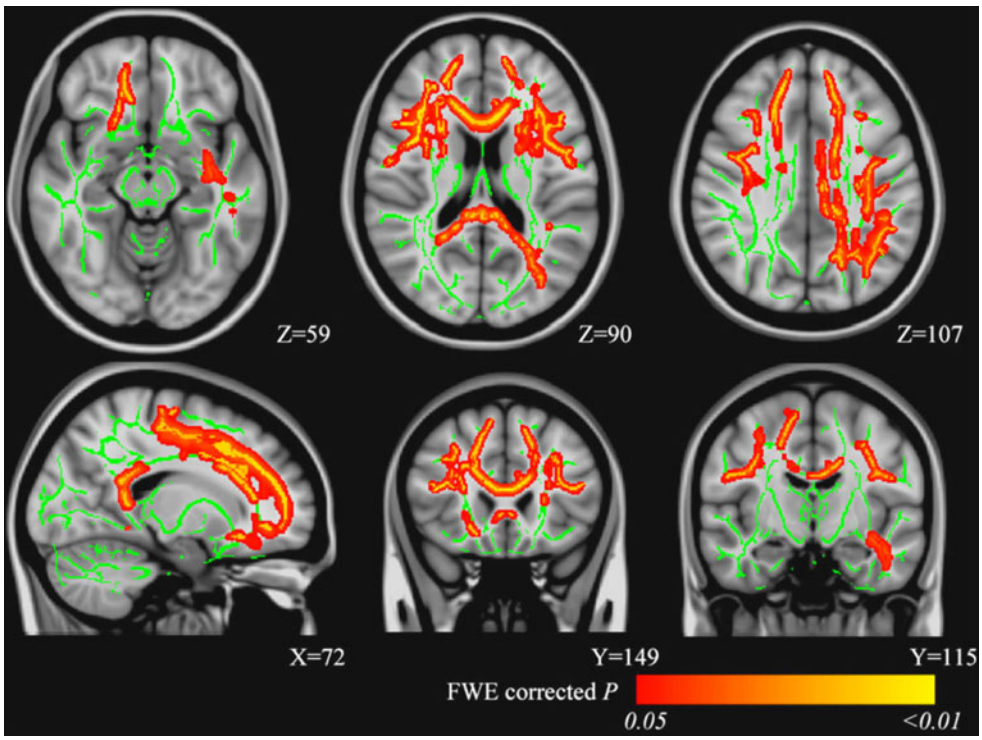

Fig. 9 Results of a tract-based spatial statistics (TBSS) analysis of mean DK values. Areas with significantly increased MDK values in subjects with hypertension compared with controls are shown in colours ranging from red to yellow ($P < 0.05$; family-wise error correction for multiple comparisons). Widespread increased MDK was observed in the hypertensive group compared with the normotensive group. Results are superimposed on the Montreal Neurological Institute 152 (MNI152) 1-mm template supplied with the FMRIB software library. The FA skeleton is shown in green. MNI space coordinates are provided in millimetres. Reproduced from Shimoji et al. [47] with permission of Springer, Inc

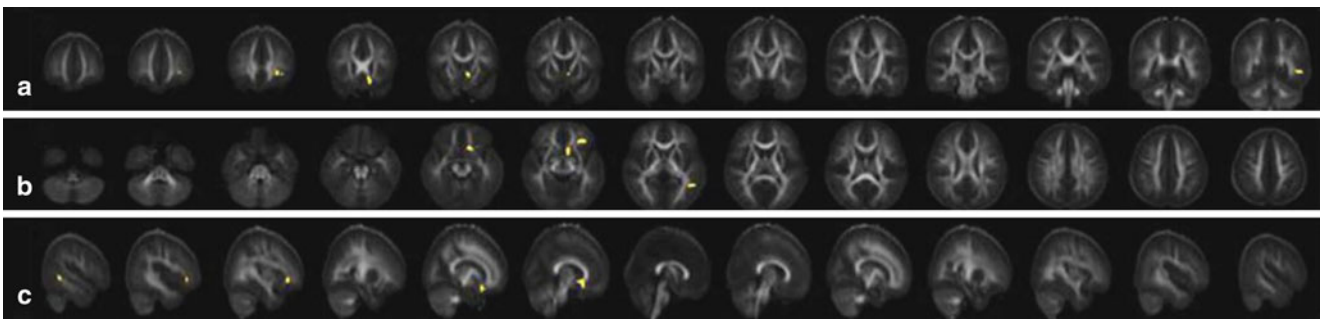

Fig. 10 Coronal (**a**), axial (**b**), and sagittal (**c**) images of FA maps. Yellow regions indicate significant differences between epilepsy and NC groups. Differences in FA regions between the two groups occurred mainly in the left cerebrum, WM and GM of the frontal and temporal lobes, the rectus, the frontal superior inferior orbital area, the caudate, the frontal gyrus, and the subcallosal gyrus. Reproduced from Zhang et al. [48] with permission of Springer, Inc

radiata, ACR; segmented temporal white matter, sTMP-WM; temporal oval, TMPo; hippocampus, H) (see Fig. 5) [37]. As shown in Fig. 6 Falangola et al. demonstrated for the first time that, relative to the C group, AD patients showed significant mean kurtosis and radial kurtosis decrease in the ACR, TMPo, sTMP-WM and gCC. Radial kurtosis was also decreased in the sPF-WM; axial kurtosis was only decreased in the ACR. When comparing C and MCI groups, authors observed decreased mean kurtosis and radial kurtosis in the PFo, and a decrease of all kurtosis metrics (MK, $K_{//}$ and $K_{\perp}$) in the ACR. These results shows that kurtosis parameters are useful additions to other diffusion measurements that may help to establish reliable biomarkers for earlier diagnosis and progression of AD [37]. Indeed, Authors reported that all DK metrics showed significant changes in the ACR between normal aging brain and patients with MCI and AD. The only DTI metric that showed a significant difference in ACR was radial diffusivity even though kurtosis metrics resulted to be more sensitive in discriminating controls from patients [37].

Van Cauter et al. demonstrated significant differences in kurtosis parameters between high-grade gliomas (HGG) and low-grade gliomas (LGG) by analyzing both axial and radial diffusivity without distinct directional dependence on higher tumor grade where increased values of kurtosis parameters probably reflect a higher degree of tissue complexity

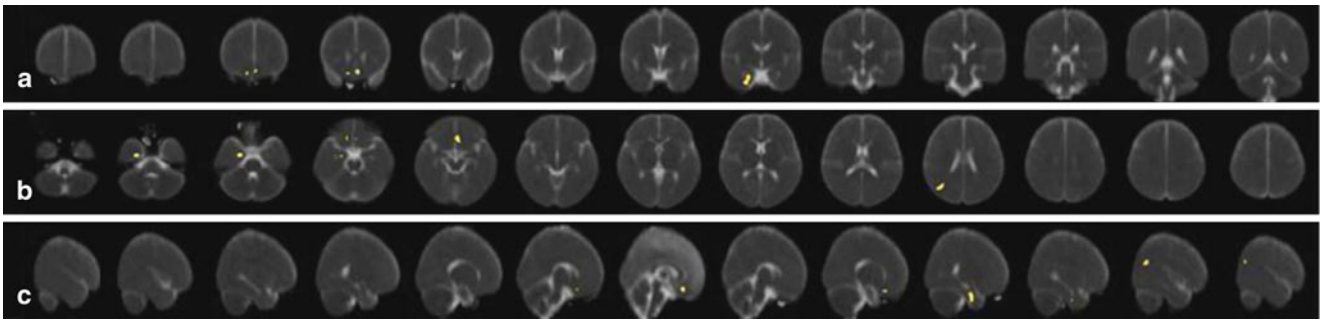

Fig. 11 Coronal (**a**), axial (**b**), and sagittal (**c**) images of MD maps. Yellow regions indicate significant differences between epilepsy and NC groups. Differences in MD regions between the two groups occurred primarily in the cerebrum bilaterally, WM and GM of the limbic lobes, the uncus, the left frontal lobe, the rectus, the right temporal lobe, the parahippocampal area, and the rectus. Reproduced from Zhang et al. [48] with permission of Springer, Inc

[44]. As shown in Fig. 7 (30-year-old woman with LGG) the MK map shows the differences between the malignant part of the tumor (high MK values, approaching the values of white matter) and the low-grade tumor (showing low MK values). Furthermore, authors found a better separation between high-grade and low-grade gliomas with MK than with conventional diffusion imaging parameters (FA and MD) as shown in Fig. 8 where parameters in solid tumor are normalized to the age-corrected value in the contralateral normal appearing white matter (normWM) [44].

DTI has been used to detect white matter damage even before the onset of cerebrovascular disease in patients with higher systolic blood pressure [45, 46]. An association between hypertension and white matter microstructural changes in middle-aged males have been found by Shimoji et al. by using DKI [47]. All the subjects included in this study were free of any visible abnormal findings during the screening MRI scan. Authors performed a tract-based spatial statistics (TBSS) analysis to investigate whole-brain FA and mean diffusional kurtosis (MDK) changes. Widespread increased MDK was observed in the hypertensive group compared with the normotensive group (Fig. 9). Further confirmation of the possible use of diffusion-based techniques to study microstructural parenchymal changes before any visible abnormal findings is appreciable with conventional MRI techniques.

Preliminary results on children with intercritical epilectiform discharges and normal brain imaging on conventional MRI suggest that DKI is sensitive for the characterization of microstructural changes of both WM and GM [48]. Figures 10, 11 and 12 show the statistically significant differences between epilepsy and normal control groups on FA, MD and MK maps respectively. Thus DKI may provide improved sensitivity and specificity for the characterization of microstructural complexities of neural tissues also in patients with epilepsy.

DKI has also been used by Lee et al. to investigate whether late-myelinating WM tracts (posterior limb of the internal capsule, PLIC; cerebral peduncle, CP) are more vulnerable to injury in medial temporal lobe epilepsy (MTLE) compared with early myelinating tracts (superior longitudinal fasciculus, SLF; inferior longitudinal fasciculus, ILF). The comparisons of the Z scores (deviation from the mean of normal controls) in the early myelinating and late-myelinating fiber tracts of the MTLE group are shown in Fig. 13. By the use of kurtosis metrics derived from DKI, Authors demonstrated that late-myelinating WM tracts are more sensitive to MTLE-related microstructural damage compared with early myelinating WM tracts, suggesting that the chronology of myelination may be a factor involved in microstructural damage caused by seizures [49].

Another grow-interest field of application are the sequelae of mild traumatic brain injury (MTBI) [50]: one of the most significant public health problems in developed countries. Combined use of DKI, DTI and Arterial Spin Labeling (ASL) look promising although there are no certain results on patients outcome prediction [51]. Moreover, DKI has been suggested as a technique that could help to better investigate patho-morphological dynamic changes following a TBI with specific references to reactive astrogliosis on an in vivo rat model studied with a high-field MR scanner (7T) [52].

Conclusions

In the last decade diffusion-weighted imaging opened a window onto what occurs in the tissues at the molecular level. DKI provides a higher-order description of the water diffusion process *in vivo* by considering along with the second order 3D diffusivity tensor (as in conventional DTI) also the fourth order 3D kurtosis tensor. The physics underling this powerful technique is complex but the DKI parameters have

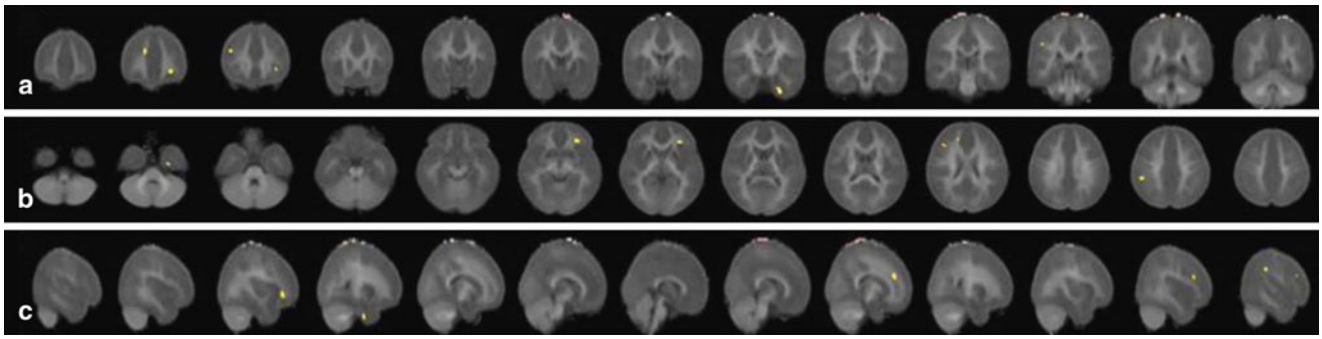

Fig. 12 Coronal (**a**), axial (**b**), and sagittal (**c**) images of MK maps. Yellow regions indicate significant differences between epilepsy and NC groups. Differences in MK regions between the two groups occurred mainly in both cerebral hemispheres, and several WM and GM regions of the frontal and parietal lobes. Reproduced from Zhang et al. [48] with permission of Springer, Inc

been found to be very sensitive in identifying some alterations which characterize many neurological diseases. These changes are appreciable with DKI even before any imaging findings through conventional imaging and in a better way than with conventional DTI. This is a relatively novel technique in which many optimal parameters require further investigations but even today it provides improved sensitivity and specificity in MR diffusion characterization of neural tissues in several brain conditions providing increasingly useful clinical data.

Appendix

In this appendix a more detailed description of the theory underlying the DK analysis is reported. As said in the main text, in DTI analyses the directionality of diffusion can be expressed by a symmetric tensor of second-order 3×3, **D**, with six independent components. In DKI analyses the directionality of the kurtosis can be expressed by a symmetric tensor of the fourth order $3 \times 3 \times 3 \times 3$, **W**. **W** being symmetric, among its 81 elements, only 15 are independent. Since the Kurtosis tensor **W** is a tensor of the fourth order, it has many eigenvalues and eigenvectors. A precise interpretation of all these parameters has not yet been defined [33]. The parameters most commonly used in the DKI are those that have a more direct physical significance and a correspondence with the diffusion tensor. The indexes of directionality of Diffusion Kurtosis can also be examined along the axial and radial directions of the diffusion tensor. In order to calculate the tensor **W** along the above-mentioned directions it must first be transformed into the coordinate system defined by the three eigenvectors (v_1, v_2, v_3) of the diffusion tensor **D**:

$$\hat{W}_{ijkl} = \sum_{i'=1}^{3}\sum_{j'=1}^{3}\sum_{k'=1}^{3}\sum_{l'=1}^{3} e_{i'i}e_{j'j}e_{k'k}e_{l'l}W_{i'j'k'l'} \tag{8}$$

where e_{ij} are the matrix elements of 3D rotation [33]. Once the values of $\hat{W}_{ijkl}$ are known the Diffusion Kurtosis parameters can be obtained by using the equations 4, 5, 6 and 7.

Since the Kurtosis represents a complex 3D structure, a rigorous formulation for MK and K_r in terms of the surface integral has been derived by Jensen [53]. For example, MK can be expressed as a surface integral of K_{app} on a unit sphere:

$$MK_s = \int K_{app}(\mathbf{g})d\Omega_g \tag{9}$$

Originally, to reconstruct the kurtosis tensor, a method that provides a non-linear fit for each of gradient direction of the following equation was proposed [54]:

$$\ln\frac{S(b,\mathbf{g})}{S_0} = -bD_{app}(\mathbf{g}) + \frac{1}{6}b^2D_{app}(\mathbf{g})^2K_{app}(\mathbf{g}) + O(b^3). \tag{10}$$

and from the knowledge of $D_{app}(\mathbf{g})$ and $K_{app}(\mathbf{g})$ it is possible to obtain the values of the elements of the tensors **D** and **W** through the equations (2) and (3). However, this was a nonlinear and two-steps procedure which also is very time-consuming. A possible way to overcome the limitations of this reconstruction algorithm derived from the fact that the equation (10) can be rewritten as:

$$\ln\frac{S(b,\mathbf{g})}{S_0} = -b\sum_{i=1}^{3}\sum_{j=1}^{3}g_ig_jD_{ij} + \frac{1}{6}b^2\left(\sum_{i=1}^{3}\left(\frac{D_{ii}}{3}\right)\right)^2 \times \sum_{i=1}^{3}\sum_{j=1}^{3}\sum_{k=1}^{3}\sum_{l=1}^{3}g_ig_jg_kg_lW_{ijkl} \tag{11}$$

and if the following setting is used:

$$\mathbf{K} = \left(\sum_{i=1}^{3}\left(\frac{D_{ii}}{3}\right)\right)^2\mathbf{W} = MD^2\mathbf{W} \tag{12}$$

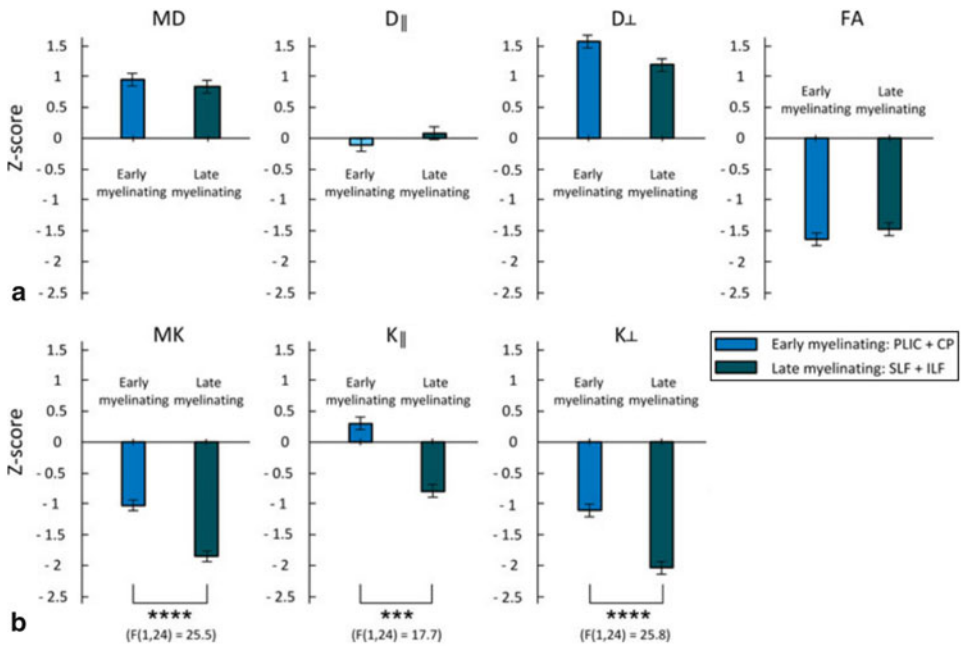

Fig. 13 Comparisons of Z scores (deviation from the mean of normal controls) in the early myelinating and late-myelinating fiber tracts of the MTLE group; $^{*}p < 0.05$, $^{**}p < 0.01$, $^{***}p < 0.001$, $^{****}p < 0.0001$, evaluated with a repeated measure ANOVA (one factor). Error bars represent the standard error. Significantly lower Z scores were observed for MK, $K_{//}$, and $K_{\perp}$ for late-myelinating ROIs, irrespective of the side of ROIs. Reproduced from Lee et al. [49] with permission of Wiley Periodicals, Inc

it becomes:

$$\ln \frac{S(b,\mathbf{g})}{S_0} = -b \sum_{i=1}^{3}\sum_{j=1}^{3} g_i g_j D_{ij} + \frac{1}{6} b^2 \sum_{i=1}^{3}\sum_{j=1}^{3}\sum_{k=1}^{3}\sum_{l=1}^{3} g_i g_j g_k g_l K_{ijkl} \quad (13)$$

This equation can be easily transformed into a set of linear equations:

$$\mathbf{Y} = \mathbf{BX} \quad (14)$$

where $\mathbf{Y}$ is a vector of N components whose elements are the logarithms of the signals:

$$\mathbf{Y} = \left[\ln S(b_1, \mathbf{g}_1) ..... \ln S(b_N, \mathbf{g}_N)\right] \quad (15)$$

$\mathbf{X}$ is a vector of 22 components whose elements are the 6 independent elements of the tensor $\mathbf{D}$, the 15 independent elements of the tensor $\mathbf{K}$ and $\ln S_0$ arranged in the following order:

$$\mathbf{X} = [D_{xx}, D_{yy}, D_{zz}, D_{xy}, D_{xz}, D_{yz}, K_{xxxx}, K_{yyyy}, K_{zzzz}, K_{xxxy}, K_{xxxz}, K_{xyyy}, K_{yyyz}, K_{xzzz}, K_{yzzz}, K_{xxyy}, K_{xxzz}, K_{yyzz}, K_{xxyz}, K_{xyyz}, K_{xyzz}, \ln S_0] \quad (16)$$

$\mathbf{B}$ is an N×22 matrix whose elements are appropriate combinations of the components of the gradient directions and b-values. In order to reduce the occurrence of estimates affected by systematic errors, the apparent diffusivity, D_{app}, and the apparent Kurtosis K_{app}, to be within biologically reasonable range [22]. For this reason, the following constraints for all directions must be satisfied for the reconstruction of the tensor:

$$D_{app}(\mathbf{g}) \geq 0 \quad (17)$$

$$K_{app}(\mathbf{g}) \geq 0 \quad (18)$$

$$K_{app}(\mathbf{g}) \leq K_{app,MAX}(\mathbf{g}) = \frac{C}{b_{max} D_{app}(\mathbf{g})} \quad (19)$$

where b_{max} is the maximum value of b-values used for the acquisition, $D_{app}(\mathbf{g})$ and $K_{app}(\mathbf{g})$ are the diffusivity and the kurtosis estimated in the direction $\mathbf{g}$. The first of these three constraints is necessary to ensure that the eigenvalues of $\mathbf{D}$ tensor are not negative. The second constraint is related to the fact that there are some limitations on the physically acceptable directional kurtoses because of biologically relevant tissue geometries [13]. Although the theoretical lower limit of K_{app} is equal to -2, for the diffusion in the brain usually it is required that $K_{app\ min}(\mathbf{g})$ is equal to 0. Regarding the third constraint, in order to ensure that $S(\mathbf{g}, b)$ is a decreasing function of b-values, the C constant is often set equal to 3. This setting is usually good in the range of b-values used for DKI data acquisitions [53]. A more strict constraint can be imposed on $K_{app}(\mathbf{g})$ by choosing a smaller constant C.

One of the objectives of this reconstruction through the algorithm is to find a good estimate of the diffusion tensor $\mathbf{D}$ and Kurtosis tensor $\mathbf{W}$ (or equivalently $\mathbf{K}$) such that the estimate of the DWI signal intensity (provided by equation

(13)), is as much as possible close to the observed values, when all constraints on diffusion and Kurtosis are met in all directions of the gradients. Previous studies shown that DKI provides more robust and unbiased data when compared to DTI [17].

Declarations All co-authors agree with the contents of the manuscript and there is no financial interest in this paper.

All human studies have been approved by the local ethics committee and have therefore been performed in accordance with the ethical standards laid down in the 1964 Declaration of Helsinki and its later amendments.

Acknowledgments The research described in this paper was supported by University of Palermo and by the Project "PON Smart Cities PON04a2_C SMART HEALTH—CLUSTER OSDH—SMART FSE - STAYWELL", and by the *"NextMR"* Project (Project Leader: A. Chincarini) funded by the Istituto Nazionale di Fisica Nucleare (INFN).

References

1. Colagrande S, Pallotta S, Vanzulli A, Napolitano M, Villari N. The diffusion parameter in magnetic resonance: physics, techniques, and semeiotics. La Radiologia Medica. 2004;109(1–2):1–16.
2. Colagrande S, Carbone SF, Carusi LM, Cova M, Villari N. Magnetic resonance diffusion–weighted imaging: extraneurological applications. La radiologia medica. 2006;111(3):392–419.
3. Cappabianca S, Iaselli F, Reginelli A, D'Andrea A, Urraro F, Grassi R, Rotondo A. Value of diffusion-weighted magnetic resonance imaging in the characterization of complex adnexal masses. Tumori. 2013;99(2):210–7.
4. Mascalchi M, Filippi M, Floris R, Fonda C, Gasparotti R, Villari N. Diffusion-weighted MR of the brain: methodology and clinical application. La Radiologia Medica. 2005;109(3):155–97.
5. Conti A, Pontoriero A, Ricciardi GK, Granata F, Vinci S, Angileri FF, Pergolizzi S, Alafaci C, Rizzo V, Quartarone A, Germanò A, Foroni RI, De Renzis C, Tomasello F. Integration of functional neuroimaging in cyberknife radiosurgery: feasibility and dosimetric results. Neurosurg Focus. 2013;34(4):E5.
6. De Nunzio G, Pastore G, Donativi M, Castellano A, Falini A. A CAD system for cerebral glioma based on texture features in DT-MR images. Nucl Instrum Methods Phys Res Sect A. 2011;648:S100–2.
7. Grinberg F, Farrher E, Ciobanu L, Geffroy F, Bihan DL, Shah NJ. Non-Gaussian Diffusion Imaging for Enhanced Contrast of Brain Tissue Affected by Ischemic Stroke. PloS one. 2014;9(2):e89225.
8. De Santis S, Gabrielli A, Palombo M, Maraviglia B, Capuani S. Non-Gaussian diffusion imaging: a brief practical review. Magn Reson Imaging. 2011;29(10):1410–6.
9. Assaf Y, Cohen Y. Non-Mono-Exponential Attenuation of Water and *N*-Acetyl Aspartate Signals Due to Diffusion in Brain Tissue. J Magn Reson. 1998;131(1):69–85.
10. Basser PJ, Jones DK. Diffusion-tensor MRI: theory, experimental design and data analysis–a technical review. NMR Biomed. 2002;15(7–8):456–67.
11. Lazar M, Jensen JH, Xuan L, Helpern JA. Estimation of the orientation distribution function from diffusional kurtosis imaging. Magn Reson Med. 2008;60(4):774–81.
12. Tuch DS, Reese TG, Wiegell MR, Makris N, Belliveau JW, Van Wedeen J. High angular resolution diffusion imaging reveals intravoxel white matter fiber heterogeneity. Magn Reson Med. 2002;48(4):577–82.
13. Jensen JH, Helpern JA, Ramani A, Lu H, Kaczynski K. Diffusional kurtosis imaging: the quantification of non-gaussian water diffusion by means of magnetic resonance imaging. Magn Reson Med. 2005;53(6):1432–40.
14. Wu EX, Cheung MM. MR diffusion kurtosis imaging for neural tissue characterization. NMR Biomed. 2010;23(7):836–48.
15. Helpern JA, Adisetiyo V, Falangola MF, Hu C, Di Martino A, Williams K, Castellanos FX, Jensen JH. Preliminary evidence of altered gray and white matter microstructural development in the frontal lobe of adolescents with attention-deficit hyperactivity disorder: a diffusional kurtosis imaging study. J Magn Reson Imaging. 2011;33(1):17–23.
16. Veraart J, Poot DHJ, Van Hecke W, Blockx I, Van der Linden A, Verhoye M, Sijbers J. More accurate estimation of diffusion tensor parameters using diffusion kurtosis imaging. Magn Reson Med. 2011;65(1):138–45.
17. Veraart J, Van Hecke W, Sijbers J. Constrained maximum likelihood estimation of the diffusion kurtosis tensor using a Rician noise model. Magn Reson Med. 2011;66(3):678–86.
18. Eichner C, Cauley SF, Cohen-Adad J, Möller HE, Turner R. Setsompop K, Wald LL. Real diffusion-weighted MRI enabling true signal averaging and increased diffusion contrast . Neuroimage. 2015;122:373–84.
19. Assaf Y, Basser PJ. Composite hindered and restricted model of diffusion (charmed) mr imaging of the human brain. Neuroimage. 2005;27(1):48–58.
20. Alexander DC, Hubbard PL, Hall MG, Moore EA, Ptito M, Parker GJM, Dyrby TB. Orientationally invariant indices of axon diameter and density from diffusion mri. Neuroimage. 2010;52(4):1374–1389.
21. Zhang H, Schneider T, Wheeler-Kingshott CA, Alexander DC. Noddi: practical in vivo neurite orientation dispersion and density imaging of the human brain. Neuroimage. 2012;61(4):1000–16.
22. Tabesh A, Jensen JH, Ardekani BA, Helpern JA. Estimation of tensors and tensor-derived measures in diffusional kurtosis imaging. Magn Reson Med. 2011;65(3):823–36.
23. Kuder TA, Stieltjes B, Bachert P, Semmler W, Laun FB. Advanced fit of the diffusion kurtosis tensor by directional weighting and regularization. Magn Reson Med. 2012;67(5):1401–11.
24. Reese TG, Heid O, Weisskoff RM, Wedeen VJ. Reduction of eddy-current-induced distortion in diffusion MRI using a twice-refocused spin echo. Magn Reson Med. 2003;49(1):177–82.
25. Pierpaoli C, Walker L, Irfanoglu MO, Barnett A, Basser P, Chang LC, Koay C, Pajevic S, Rohde G, Sarlls J, Wu M. TORTOISE: an integrated software package for processing of diffusion MRI data. Proceedings 18th Scientific Meeting, International Society for Magnetic Resonance in Medicine. 2010.
26. Collura G, Marrale M, Toschi N, Gagliardo C, Midiri M, Brai M. Sviluppo di un software per l'analisi di immagini di Diffusion Kurtosis Imaging. Proceedings AIRP - Atti del XXXVI Convegno Nazionale di Radioprotezione, Palermo, 18–20 settembre 2013. 2013.
27. Lätt J, Nilsson M, Wirestam R, Ståhlberg F, Karlsson N, Johansson M, Sundgren PC, van Westen D. Regional values of diffusional kurtosis estimates in the healthy brain. J Magn Reson Imaging. 2013;37(3):610–8.
28. Beaulieu C. The basis of anisotropic water diffusion in the nervous system–a technical review. NMR Biomed. 2002;15(7–8):435–55.
29. Basser PJ, Pierpaoli C. Microstructural and physiological features of tissues elucidated by quantitative-diffusion-tensor MRI. J Magn Reson Series B. 1996;111(3):209–19.
30. Chincarini A, Bosco P, Gemme G, Morbelli S, Arnaldi D, Sensi F, Solano I, Amoroso N, Tangaro S, Longo R, Squarcia S, Nobili F. Alzheimers disease markers from structural MRI and FDG-PET brain images. Eur Phys J Plus. 2012;127(11):1–16.

31. Nobili F, Arnaldi D, Roccatagliata L, Chincarini A, Accardo J, Picco A, Ferrara M, Buschiazzo A, Morbelli S. Neuroimaging Findings in Mild Cognitive Impairment. PET and SPECT Neurol. 2014;271–307.
32. Yablonskiy DA, Bretthorst GL, Ackerman JJH. Statistical model for diffusion attenuated MR signal. Magn Reson Med. 2003;50(4):664–9.
33. Hui ES, Cheung MM, Qi L, Wu EX. Towards better MR characterization of neural tissues using directional diffusion kurtosis analysis. Neuroimage. 2008;42(1):122–34.
34. Sevick RJ, Kucharczyk J, Mintorovitch J, Moseley ME, Derugin N, Norman D. Diffusion-weighted MR imaging and T2-weighted MR imaging in acute cerebral ischaemia: comparison and correlation with histopathology. Acta Neurochir Suppl (Wien). 1990;51:210–2.
35. Hu C, Jensen JH, Falangola MF, Helpern JA. CSF partial volume effect for diffusion kurtosis imaging. Proceedings 16th Scientific Meeting, International Society for Magnetic Resonance in Medicine. 2008.
36. Hui ES, Fieremans E, Jensen JH, Tabesh A, Feng W, Bonilha L, Spampinato MV, Adams R, Helpern JA. Stroke assessment with diffusional kurtosis imaging. Stroke. 2012;43(11):2968–73.
37. Falangola MF, Jensen JH, Tabesh A, Hu C, Deardorff RL, Babb JS, Ferris S, Helpern JA. Non-Gaussian diffusion MRI assessment of brain microstructure in mild cognitive impairment and Alzheimers disease. Magn Reson Imaging. 2013;31(6):840–6.
38. Guo AC, MacFall JR, Provenzale JM. Multiple sclerosis: diffusion tensor mr imaging for evaluation of normal-appearing white matter 1. Radiology. 2002;222(3):729–36.
39. Rovaris M, Agosta F, Pagani E, Filippi M. Diffusion tensor mr imaging. Neuroimaging Clin N Am. 2009;19(1):37–43.
40. Werring DJ, Brassat D, Droogan AG, Clark CA, Symms MR, Barker GJ, MacManus DG, Thompson AJ, Miller DH. The pathogenesis of lesions and normal-appearing white matter changes in multiple sclerosis a serial diffusion mri study. Brain. 2000;123(8):1667–76.
41. Scanderbeg AC, Tomaiuolo F, Sabatini U, Nocentini U, Grasso MG, Caltagirone C. Demyelinating plaques in relapsing-remitting and secondary-progressive multiple sclerosis: assessment with diffusion mr imaging. AJNR Am Neuroradiol. 2000;21(5):862–8.
42. Kamagata K, Tomiyama H, Motoi Y, Kano M, Abe O, Ito K, Shimoji K, Suzuki M, Hori M, Nakanishi A, et al. Diffusional kurtosis imaging of cingulate fibers in Parkinson disease: comparison with conventional diffusion tensor imaging. Magn Reson Imaging. 2013;31(9):1501–6.
43. Wang J-J, Lin W-Y, Lu C-S, Weng Y-H, Ng S-H, Wang C-H, Liu H-L, Hsieh R-H, Wan Y-L, Wai Y-Y. Parkinson disease: diagnostic utility of diffusion kurtosis imaging. Radiology. 2011;261(1):210–7.
44. Van Cauter S, Veraart J, Sijbers J, Peeters RR, Himmelreich U, De Keyzer F, Van Gool SW, Van Calenbergh F, De Vleeschouwer S, Van Hecke W, Sunaert S. Gliomas: diffusion kurtosis MR imaging in grading. Radiology. 2012;263(2):492–501.
45. Gons RAR, de Laat KF, van Norden AGW, van Oudheusden LGB, van Uden IWM, Norris DG, Zwiers MP, de Leeuw FE. Hypertension and cerebral diffusion tensor imaging in small vessel disease. Stroke. 2010;41(12):2801–6.
46. MacLullich AMJ, Ferguson KJ, Reid LM, Deary IJ, Starr JM, Seckl JR, Bastin ME, Wardlaw JM. Higher systolic blood pressure is associated with increased water diffusivity in normal-appearing white matter. Stroke. 2009;40(12):3869–71.
47. Shimoji K, Uka T, Tamura Y, Yoshida M, Kamagata K, Hori M, Motoi Y, Watada H, Kawamori R, Aoki S. Diffusional kurtosis imaging analysis in patients with hypertension. Jpn J Radiol. 2014;32(2):98–104.
48. Zhang Y, Yan X, Gao Y, Xu D, Wu J, Li Y. A preliminary study of epilepsy in children using diffusional kurtosis imaging. Clin Neuroradiol. 2013;23(4):293–300.
49. Lee C-Y, Tabesh A, Benitez A, Helpern JA, Jensen JH, Bonilha L. Microstructural integrity of early-versus late-myelinating white matter tracts in medial temporal lobe epilepsy. Epilepsia. 2013;54(10):1801–9.
50. Solarino M, Iovane A, Sutera R. Principi di diagnostica per immagini in medicina dello sport, chapter 18, pages 163–80. EdiSES, 1 edition, 2014. *Trauma cranico nello sport*. by Gagliardo, C and La Tona, G and Iovane, A.
51. Grossman EJ, Jensen JH, Babb JS, Chen Q, Tabesh A, Fieremans E, Xia D, Inglese M, Grossman RI. Cognitive impairment in mild traumatic brain injury: a longitudinal diffusional kurtosis and perfusion imaging study. AJNR Am J Neuroradiol. 2013;34(5):951–7.
52. Zhuo J, Xu S, Proctor JL, Mullins RJ, Simon JZ, Fiskum G, Gullapalli RP. Diffusion kurtosis as an in vivo imaging marker for reactive astrogliosis in traumatic brain injury. Neuroimage. 2012;59(1):467–77.
53. Jensen JH, Helpern JA. MRI quantification of non-Gaussian water diffusion by kurtosis analysis. NMR Biomed. 2010;23(7):698–710.
54. Lu H, Jensen JH, Ramani A, Helpern JA. Three-dimensional characterization of non-gaussian water diffusion in humans using diffusion kurtosis imaging. NMR Biomed. 2006;19(2):236–47.